Iryna Hlushchenko and Pirta Hotulainen*

Chemical LTD, but not LTP, induces transient accumulation of gelsolin in dendritic spines

Abstract: Synaptic plasticity underlies central brain functions, such as learning. Ca^{2+} signaling is involved in both strengthening and weakening of synapses, but it is still unclear how one signal molecule can induce two opposite outcomes. By identifying molecules, which can distinguish between signaling leading to weakening or strengthening, we can improve our understanding of how synaptic plasticity is regulated. Here, we tested gelsolin's response to the induction of chemical long-term potentiation (cLTP) or long-term depression (cLTD) in cultured rat hippocampal neurons. We show that gelsolin relocates from the dendritic shaft to dendritic spines upon cLTD induction while it did not show any relocalization upon cLTP induction. Dendritic spines are small actin-rich protrusions on dendrites, where LTD/LTP-responsive excitatory synapses are located. We propose that the LTD-induced modest – but relatively long-lasting – elevation of Ca^{2+} concentration increases the affinity of gelsolin to F-actin. As F-actin is enriched in dendritic spines, it is probable that increased affinity to F-actin induces the relocalization of gelsolin.

Keywords: actin cytoskeleton; neurons; synaptic plasticity.

Introduction

Synaptic plasticity, the strengthening and weakening of synapses, is one of the key cellular and molecular mechanisms underlying information processing in the brain. Long-term potentiation (LTP) strengthens synapses and is considered a molecular mechanism underlying learning. In contrast, long-term depression (LTD) weakens synapses, even depletes them, and is crucial for developmental and experience-based network refinement (Holtmaat and Svoboda, 2009; Chen et al., 2014). Precise balance of LTP and LTD is important for normal brain function. The shift of balance to either side can lead to numerous neurological disorders (Hanson and Madison, 2010). While much attention has been given to synapse strengthening, the mechanisms and functional implications of synapse weakening have been neglected.

LTP and LTD are both occurring at excitatory synapses. Most post-synaptic terminals of excitatory synapses exist on small bulbous structures on neuronal dendrites known as dendritic spines. Both LTP and LTD rely on Ca^{2+} influx through N-methyl-D-aspartate (NMDA) receptors (Yang et al., 1999). The earlier activation history of a synapse, frequency, and total time of stimulation, as well as the degree of the calcium concentration elevation in the spine will determine whether the synapse will be strengthened or weakened (Abraham, 2008). The morphological and structural changes induced by synapse activation are mainly controlled by the actin cytoskeleton. Synaptic stimulation rapidly changes actin dynamics (Star et al., 2002; Okamoto et al., 2004) and many actin regulators have been shown to play roles in both LTP and LTD. Induction of LTP triggers a cascade of events involving Ca^{2+} signaling and regulation of actin-binding proteins such as CaMKII, cofilin, Aip1, Arp2/3, α-actinin, profilin and drebrin (Hlushchenko et al., 2016). In LTD, the calcium-dependent phosphatase calcineurin is activated, leading to the activation of cofilin and F-actin loss in dendritic spines (Halpain et al., 1998; Okamoto et al., 2004; Zhou et al., 2004; Hayama et al., 2013).

Gelsolin (GSN) is a multifunctional actin-binding protein that can bind both G- and F-actin, sever and cap the filaments and even nucleate actin polymerization. Gelsolin is expressed ubiquitously, including in the brain (Tanaka and Sobue, 1994; Li et al., 2012; Nag et al., 2013). It can be regulated by the intracellular pH, Ca^{2+} concentration and phosphoinositide binding (Kinosian et al., 1998). Gelsolin is composed of six domains (G1–G6) and each of these domains contains a Ca^{2+} binding site. In its resting state (low Ca^{2+} concentration), gelsolin is mostly free in the cytosol but also partially bound to phosphoinositides on the plasma membrane. Upon increase in Ca^{2+} concentration, gelsolin's affinity to F-actin increases, leading to binding of actin filaments followed by actin filament severing (Forscher, 1989; Li et al., 2010). Due to

*Corresponding author: Pirta Hotulainen,** Minerva Foundation Institute for Medical Research, Biomedicum Helsinki 2U, Tukholmankatu 8, FI-00290 Helsinki, Finland, e-mail: pirta.hotulainen@helsinki.fi
Iryna Hlushchenko: Minerva Foundation Institute for Medical Research, Biomedicum Helsinki 2U, Tukholmankatu 8, FI-00290 Helsinki, Finland
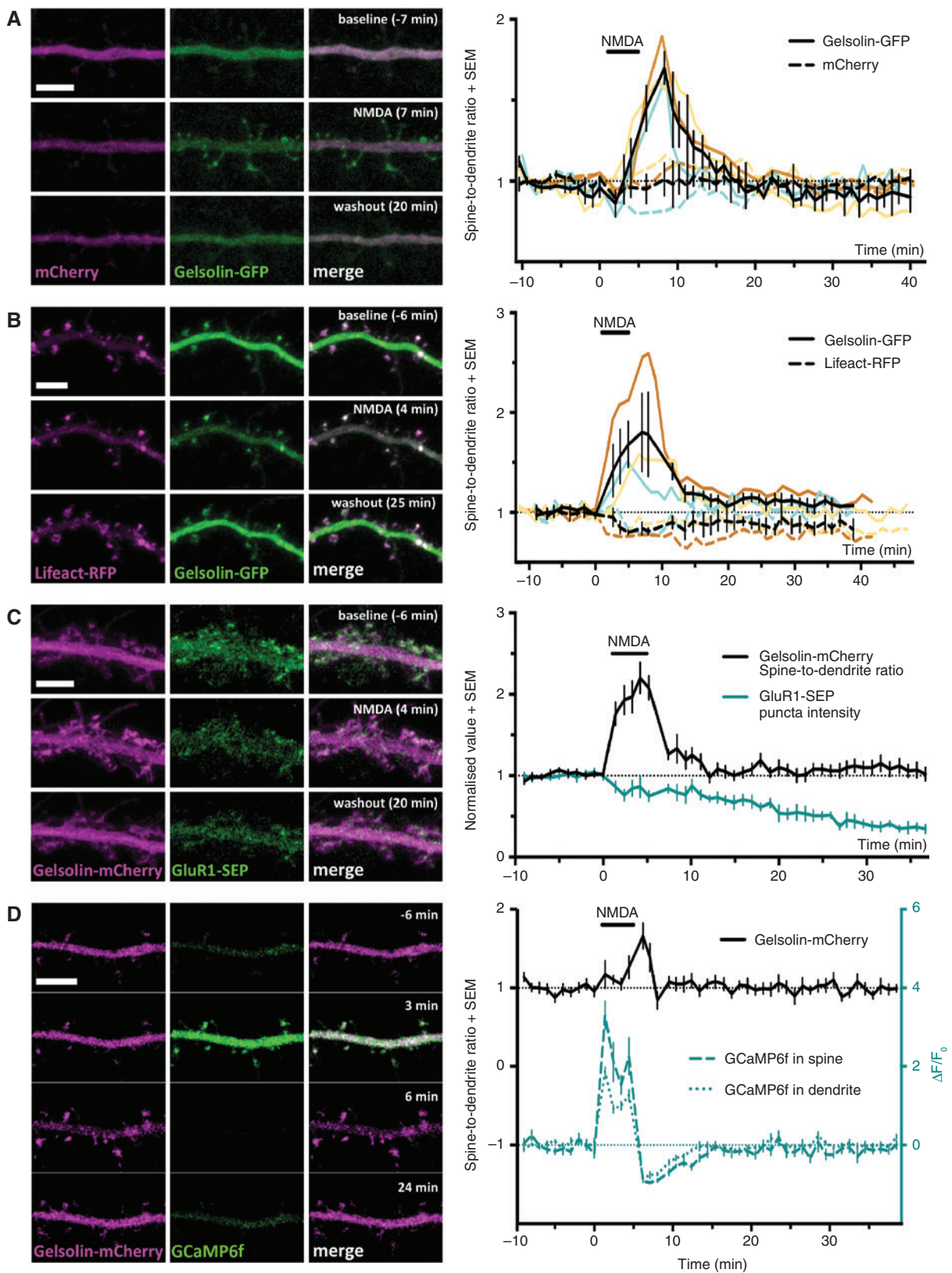
its regulation, and because it is one of the most potent actin-severing factors, gelsolin has been considered as a potential player in dendritic spine remodeling during synaptic plasticity (Furukawa et al., 1997; Hlushchenko et al., 2016). However, only a few studies have experimentally addressed the function of gelsolin in dendritic spine

Figure 1: Gelsolin accumulates transiently in dendritic spines upon chemical LTD induction.
(A) The images show the representative maximum projections of confocal Z-stacks for a live neuron expressing gelsolin-GFP (in green) along with mCherry (in magenta). From top to bottom, the three timepoints are represented: baseline, right after cLTD induction, and at the end of the protocol. Scale bar, 5 μm. The traces demonstrate how the spine-to-dendrite fluorescence intensity ratio changes over the course of cLTD stimulation, which reflects the protein distribution between the spines and dendrite. Each of the colored traces corresponds to one of the three independent experiments and is a mean of the spine-to-dendrite ratio of 10 spines for each experiment. The black traces are the average of the three already-mentioned experiments (in total n = 30 spines from three cells). (B) The images show the representative maximum projections of confocal Z-stacks for a live neuron expressing gelsolin-GFP (in green) along with Lifeact-RFP (in magenta). From top to bottom the three timepoints are represented: baseline, right after cLTD induction, and at the end of the protocol. Scale bar, 5 μm. The traces demonstrate how the spine-to-dendrite fluorescence intensity ratio changes over the course of cLTD stimulation, which reflects the protein distribution between spines and the dendrite. Each of the colored traces corresponds to one of the three experiments and is a mean of spine-to-dendrite ratio of 10 spines for each experiment. The black traces are the average of the three already-mentioned experiments (in total n = 30 spines from three cells). (C) The images show the representative maximum projections of confocal Z-stacks for a live neuron expressing gelsolin-mCherry (in magenta) along with GluA1-SEP (in green). From top to bottom the three timepoints are represented: baseline, right after cLTD induction, and at the end of the protocol. Scale bar, 5 μm. The black trace demonstrates how the spine-to-dendrite fluorescence intensity ratio for gelsolin-mCherry changes over the course of cLTD stimulation in one experiment and is a mean of ratios of 10 spines from one cell. The cyan trace represents a mean of the normalized values of eight GluA1-SEP puncta intensities from the already-mentioned cell. (D) The images show the representative maximum projections of confocal Z-stacks for a live neuron expressing gelsolin-mCherry (in magenta) along with GCaMP6f (in green). From top to bottom the four timepoints are represented: baseline, a Ca^{2+} concentration elevation during NMDA application, gelsolin redistribution right after cLTD induction, and at the end of the protocol. Scale bar, 5 μm. The black trace demonstrates how the spine-to-dendrite fluorescence intensity ratio for gelsolin-mCherry changes over the course of cLTD stimulation in one experiment and is a mean of ratios of 10 spines from the one cell. The cyan traces represent a mean fluorescence intensity change ($F–F_0/F_0$) of GCaMP6f in the same 10 spines and adjacent dendrites.

morphogenesis or in synaptic plasticity. Gelsolin overexpression in days-in-vitro (DIV) 12 neuronal cultures, decreased – while knock-down increased – the length of dendritic protrusions (Hu and Hsueh, 2014). The change in spine morphology upon gelsolin overexpression was observed only in the presence of Ca^{2+}, suggesting that gelsolin-induced modulation of spines requires Ca^{2+} (Hu and Hsueh, 2014). Primary hippocampal neurons cultured from mice lacking gelsolin exhibited decreased actin filament depolymerization after exposure to glutamate (Furukawa et al., 1997). Star et al. showed that gelsolin is needed for actin stabilization after low frequency stimulation (Star et al., 2002) and Zhao had found that gelsolin can accumulate in dendritic spines upon activation of glutamate receptors (Zhao, 2003). On the other hand, Morishita et al. reported that LTD of postsynaptic currents was normally maintained in *gsn* knockout mice (Morishita et al., 2005). Thus, it seems that gelsolin is involved in Ca^{2+}-dependent modulation of dendritic spine morphology, and this might be related to LTD, but details in this picture are still far from clear.

In this study, we tested whether gelsolin responds to the induction of chemical LTP (cLTP) or LTD (cLTD) in cultured rat hippocampal neurons. We show that gelsolin relocates to dendritic spines upon cLTD induction, but does not exhibit any relocalization upon cLTP induction. This result supports the evidence of gelsolin being involved in LTD formation. Based on these results, gelsolin has a unique ability to distinguish between LTD and LTP.

Understanding the molecular mechanisms underlying this ability would facilitate our understanding on how cells can separate the signaling cascades leading to LTP or LTD.

Results

Gelsolin accumulates transiently in dendritic spines upon chemical LTD induction

To test whether gelsolin responds to LTD induction, we treated DIV 18–21 neurons simultaneously expressing gelsolin-GFP and mCherry with a solution containing 50 μM NMDA for 4 min. The live imaging of these neurons revealed that already during NMDA application, diffusely distributed gelsolin started to accumulate in dendritic spines. The accumulation peaked 8 min after starting the NMDA application and was sustained significantly above the baseline for 7 min, on average (timepoints 7–13 min). Simultaneously followed mCherry distribution did not change (Figure 1A).

Gelsolin severs and caps F-actin and LTD induction has been shown to shift the F-actin/G-actin equilibrium towards G-actin, resulting in a loss of postsynaptic actin (Okamoto et al., 2004). Thus, to monitor whether gelsolin re-localization parallels with the decrease in postsynaptic F-actin, we repeated the previous experiments in 18–22 DIV hippocampal neurons expressing gelsolin-GFP and
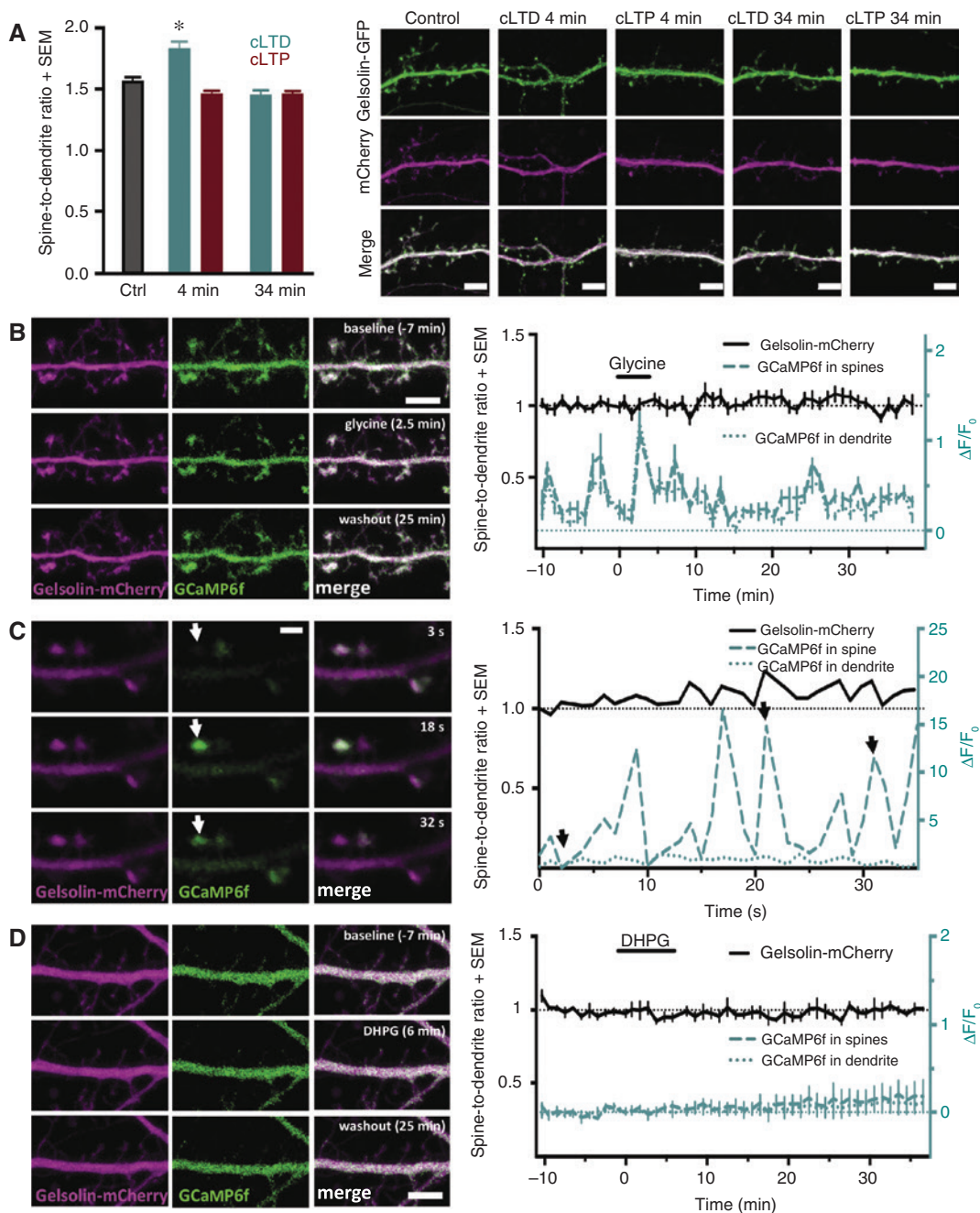
Lifeact-RFP. The Lifeact probe is a 17-amino-acid peptide, which binds mainly F-actin (and not G-actin) in cells (Riedl et al., 2008). In the baseline recording, Lifeact-RFP was highly enriched in dendritic spines, whereas gelsolin was uniformly distributed through dendritic shaft and spines (Figure 1B). Consistent with previous experiments, gelsolin accumulated in dendritic spines and showed a high co-localization with F-actin upon NMDA application (Figure 1B). The onset of the accumulation of gelsolin in dendritic spines was also correlated with a 20% decrease in Lifeact-RFP signal in dendritic spines. The decrease in F-actin accumulation in spines was statistically significant

from 3 min after starting NMDA application until the end of recording (40 min) (Figure 1B).

The main cellular mechanism of LTD is the decrease in the number of postsynaptic AMPA-type glutamate receptors (AMPAR) (Malinow and Malenka, 2002). To control the efficiency of the used cLTD protocol, we repeated cLTD induction protocol in the 3-week-old cultured neurons expressing gelsolin-mCherry and GluR1-SEP. The superecliptic pHluorin (SEP) marker is a pH-sensitive form of GFP (Miesenböck et al., 1998). The resulting receptor should display fluorescence when on the surface membrane (which exposes SEP to a neutral environment)

Figure 2: Gelsolin is enriched in spines upon cLTD but not cLTP induction.
(A) For quantification of protein localization, the ratio of gelsolin-GFP fluorescence in the spine to that in the dendrite was normalized to the intensity of mCherry fluorescence. Untreated cells were used as a control. The analysis revealed the higher localization of gelsolin-GFP to dendritic spines after cLTD induction but not cLTP induction. Spine-to-dendrite fluorescence intensity ratios: control: 1.57 ($n = 8$ cells, 160 spines), cLTD 0 min: 1.84 ($n = 8$ cells, 145 spines), cLTP 0 min: 1.47 ($n = 12$ cells, 240 spines), cLTD 30 min: 1.47 ($n = 5$ cells, 90 spines), cLTP 30 min: 1.46 ($n = 8$ cells, 160 spines). Data gathered from one experiment. *$p < 0.01$ as determined by the Kruskal-Wallis nonparametric test. The images show the representative maximum projections of confocal Z-stacks for a fixed neuron at DIV21 expressing gelsolin-GFP (in green) along with mCherry (in magenta). From left to right the five conditions are represented: control, right after cLTD induction, right after cLTP induction (time point 4-min), 30 min after cLTD induction, and 30 min after cLTP induction (time point 34-min). The intensity of white coloration in the image reflects the degree of colocalization. Scale bar, 5 μm. (B) The images show the representative maximum projections of confocal Z-stacks for a live neuron expressing gelsolin-mCherry (in magenta) along with GCaMP6f (in green). From top to bottom the three timepoints are represented: baseline, a Ca^{2+} concentration elevation at the end of glycine application, and at the end of the protocol. Scale bar, 5 μm. The black trace demonstrates how the spine-to-dendrite fluorescence intensity ratio for gelsolin-mCherry changes over the course of cLTP stimulation in one experiment and is a mean of ratios of eight spines from one neuron. The cyan traces represent a mean fluorescence intensity change ($F-F_0/F_0$) of GCaMP6f in the same eight spines and adjacent dendrites. (C) The images show the representative maximum projections of confocal Z-stacks for a live neuron expressing gelsolin-mCherry (in magenta) along with GCaMP6f (in green). From top to bottom the three timepoints are represented: the baseline, the end of DHPG application, and at the end of the protocol. Scale bar, 5 μm. The black trace demonstrates how the spine-to-dendrite fluorescence intensity ratio for gelsolin-mCherry changes over the course of cLTP stimulation in three experiments and is a mean of ratios of 30 spines. The cyan traces represent a mean fluorescence intensity change ($F-F_0/F_0$) of GCaMP6f in the same 30 spines and adjacent dendrites. (D) The images show the segment of dendritic branch of a live neuron expressing gelsolin-mCherry (in magenta) along with GCaMP6f (in green) exhibiting spontaneous activity. From top to bottom the three timepoints are represented: low Ca^{2+} concentration in the one measured spine, a high Ca^{2+} concentration, and medium Ca^{2+} concentration. Scale bar, 2 μm. The black trace demonstrates how the spine-to-dendrite fluorescence intensity ratio for gelsolin-mCherry changes over the course of recording in one spine. The cyan traces represent a fluorescence intensity change ($F-F_0/F_0$) of GCaMP6f in the same spine and adjacent dendrite.

and should be mostly non-fluorescent when trapped in intracellular compartments (which have a lower pH) (Anderson et al., 1984). Therefore, only AMPA receptors on the cell surface are visualized as the endocytosed receptor subunits exposed to acidic pH are not emitting any signal. Earlier reports have shown a gradual decrease in surface AMPARs (GluA1 in this case) 7–10 min after starting NMDA application and the decreased level was kept at a low level until the end of observation (>30 min) (Sanderson et al., 2011; Fujii et al., 2018). Our experiment showed that the signal obtained from surface GluR1 in dendritic spines started to decrease upon the application of NMDA. At the same time, simultaneously recorded gelsolin fluorescence accumulated in dendritic spines similar to earlier experiments (Figure 1C). Decrease in surface AMPA receptor intensity continued in a linear fashion throughout the time of recording (35 min). At 35 min after the onset of application it was 40% of the baseline value (Figure 1C).

NMDA application-induced cLTD causes transient increase in Ca^{2+} concentration in spines (Yang et al., 1999). To further check the functionality of the used cLTD protocol, we repeated the same experiment with neurons expressing gelsolin-mCherry and the calcium indicator GCaMP6f. GCaMP6f is an ultrasensitive protein calcium sensor, increasing its fluorescence intensity upon increase in Ca^{2+} concentration. Imaging with GCaMP6f showed a fast elevation in Ca^{2+} concentration in dendritic shafts and spines, which lasted throughout the NMDA application. The increase in gelsolin accumulation followed

immediately after the Ca^{2+} concentration increase, indicating that such Ca^{2+} concentration increase could activate gelsolin to bind F-actin and F-actin enrichment in spines would then recruit gelsolin to spines (Figure 1D).

Taken together, these experiments showed that cLTD induced by a 4-min NMDA application results in immediate increase in Ca^{2+} concentration followed by slower decrease in cell surface expression of GluR1, re-localization of gelsolin from dendritic shaft to spines, and reduced accumulation of F-actin in dendritic spines.

Gelsolin is enriched in spines upon cLTD but not cLTP induction

Both LTD and LTP require an elevation in Ca^{2+} concentration. LTP induction typically leads to a large but short increase, whereas LTD stimulus induces a modest and clearly longer-lasting increase in Ca^{2+} concentration. If just any type of increase in Ca^{2+} concentration would induce gelsolin relocalization from the shaft to spines, then both cLTD and cLTP inductions should induce gelsolin relocalization. Thus, we compared the changes in gelsolin localization upon cLTD and cLTP induction in fixed cells. We first induced chemical LTD or LTP (Lu et al., 2001) in DIV 21 hippocampal neurons, and then fixed them immediately after chemical stimulation (4-min time point) or 30 min after the washout (34-min time point) (Figure 2A). Gelsolin enrichment in
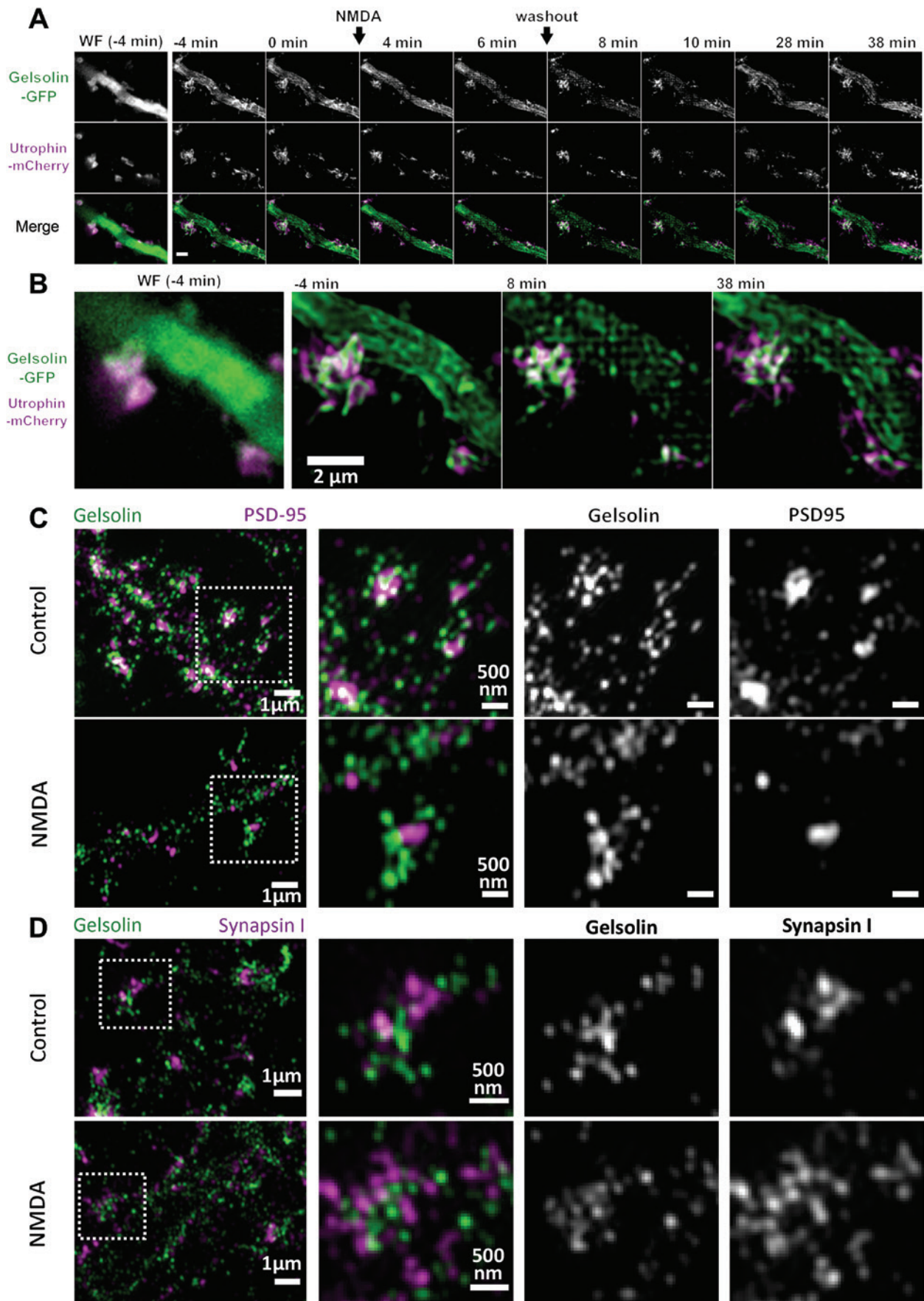
Figure 3: Gelsolin co-localizes with actin filaments but not with synaptic structures.
(A) The images demonstrate the maximum projection of 3D SIM reconstructions for a live DIV21 neuron expressing gelsolin-GFP along with Utrophin-mCherry. The neuron was treated with 50 μM NMDA for 4 min. Scale bar, 2 μm. (B) Close-up view of the few frames from panel (A). (C) The immunostaining of DIV28 neurons with antibodies against gelsolin and the post synaptic marker PSD-95. The upper panel shows control neurons and the lower panel shows neurons fixed after treatment with NMDA. (D) The immunostaining of DIV28 neurons with antibodies against gelsolin and the pre-synaptic marker Synapsin-I. The upper panel shows control neurons and the lower panel shows neurons fixed after treatment with NMDA.

spines was observed immediately after cLTD induction, whereas induction of cLTP did not affect gelsolin distribution. Similar to live experiments shown in Figure 1, gelsolin enrichment in dendritic spines was lost 30 min after the washout. To ensure that we just did not miss the timepoint when gelsolin would relocate with LTP induction, we repeated the live experiments shown in Figure 1D, with LTP protocol. These results showed that despite the short increase in Ca²⁺ concentration, gelsolin did not change its distribution (Figure 2B).

We further tested whether spontaneous activity-induced increase in Ca²⁺ concentration relocates overexpressed gelsolin-mCherry from shaft to spines. Although Ca²⁺ concentration shortly increased at specific spines, we did not detect any change in gelsolin localization (Figure 2C). We further tested whether a Ca²⁺-independent LTD protocol affects gelsolin's distribution. We induced cLTD by applying mGluR agonist dihydroxyphenylglycine (DHPG) to the cells for 7 min as described in (Sanderson et al., 2011) (Figure 2D). Hippocampal mGluR-LTD requires Gαq but occurs independently of postsynaptic Ca²⁺ increases or IP3-sensitive Ca²⁺ stores (Fitzjohn et al., 2001; Kleppisch et al., 2001; Moult et al., 2006). mGluR agonist treatment did not affect gelsolin distribution indicating that LTD-induced redistribution needs increase in Ca²⁺ concentration.

Together, this data indicates that Ca²⁺-dependent cLTD – but not Ca²⁺-independent cLTD, cLTP or spontaneous activity – induce transient accumulation of gelsolin in spines.

SIM imaging shows that gelsolin co-localizes with actin filaments but not with synaptic structures

During our initial live imaging experiments we have noticed that gelsolin often accumulates in the central area of the dendritic spine, however, with the resolution of conventional light microscopy it is hard to make conclusions about sub-spine distribution of proteins. To explore this further and also to test the possible mechanisms of gelsolin recruitment to spines upon NMDA treatment we have repeated our live experiments using structured illumination super resolution microscopy (SIM). Based on the fact

that high Ca²⁺ concentration increases gelsolin's affinity to actin filaments (Kinosian et al., 1998), we hypothesized that the relatively long increase in Ca²⁺ concentration detected in cLTD induction (Figure 1D) opens the structure of gelsolin, leading to binding to F-actin. As F-actin is enriched in dendritic spines, and hardly visible in the dendritic shaft, binding to actin would then recruit gelsolin to spines upon NMDA treatment. Thus, we followed gelsolin-GFP and utrophin-mCherry (a fluorescent marker for F-actin; Burkel et al., 2007) at DIV 21 neurons. Similar to the live experiments shown in Figure 1, NMDA treatment induced a transient loss of gelsolin from the dendritic shaft and accumulation in dendritic spines (Figure 3A, B). Although SIM does not allow quantification of the changes in fluorescent intensity we can judge the amount of gelsolin co-localizing with F-actin based on the reconstructed structure of dendrite and spines. Upon cLTD stimulation, gelsolin distribution was transiently more similar to F-actin distribution. Based on these experiments, recruitment of gelsolin through a Ca²⁺-induced increase in affinity to F-actin is a possible mechanism. However, there might also be additional mechanisms to recruit gelsolin to spines upon NMDA treatment.

Next, we tested whether gelsolin co-localizes with synaptic markers in spines and whether the enhanced binding to the receptor area could explain the accumulation of gelsolin in spines upon NMDA treatment. Here, we used DIV28 fixed low density neurons stained against gelsolin and synaptic markers. SIM imaging revealed that gelsolin is located close to synapses, marked by anti-PSD-95 antibody (Figure 3C). PSD-95 is a scaffolding protein for postsynaptic density. Although gelsolin was located close to synaptic structures, it seldom co-localized with synaptic markers. These results were confirmed using the pre-synaptic marker synapsin (Figure 3D). NMDA treatment did not change the distribution of gelsolin relative to PSD-95 or synapsin stainings (Figure 3C, D).

Gelsolin overexpression has a minor effect on spine density, morphology or dynamics

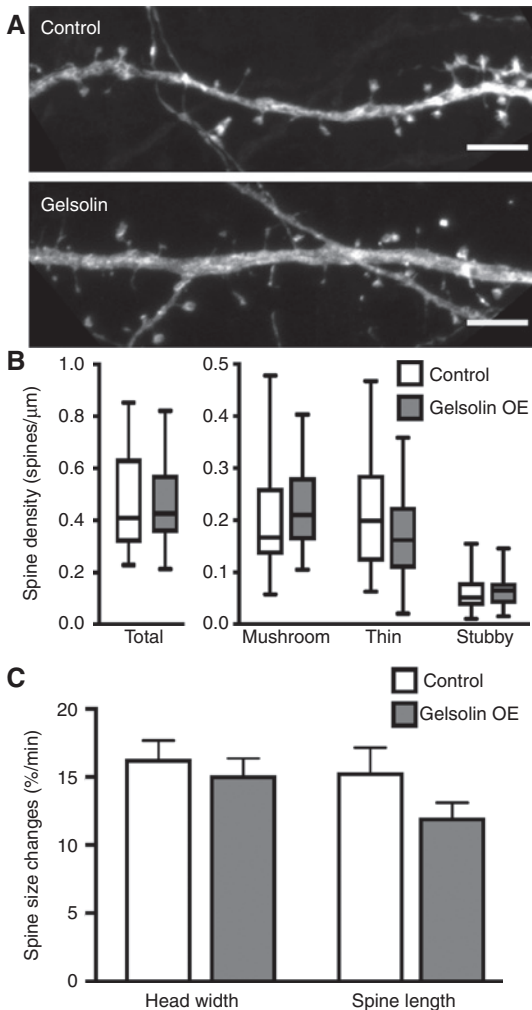To test whether an increased gelsolin expression level affects dendritic spine density or morphology at resting

Figure 4: Gelsolin overexpression has a minor effect on spine density, morphology or dynamics.
(A) The images show the representative maximum projections of confocal Z-stacks for fixed neurons at DIV15 expressing gelsolin-GFP (gelsolin) or EGFP (control). Scale bar, 4 μm. (B) Quantification of dendritic spine density calculated as number of spines per 1 μm of dendrite. Proportions of thin, mushroom, and stubby spines were as follows: control: thin = 0.20, mushroom = 0.21, stubby = 0.04, total density = 0.45 spines/μm (n = 25 neurons, 1271 spines, 2842 μm dendrite) gelsolin: thin = 0.18, mushroom = 0.22, stubby = 0.05, total density = 0.45 spines/μm (n = 25 neurons, 1147 spines, 2701 μm dendrite). Data is pooled from five experiments. Center lines of box plots show the medians; box limits indicate the 25th and 75th percentiles as determined by 'Prism 7' software; whiskers indicate maximum and minimum values. No significant differences between groups were detected by the Kruskal-Wallis nonparametric test. (C) Quantification of dendritic spine motility. Confocal Z-stacks of dendritic branches were acquired at 1-min intervals. Analysis of spine motility was performed by measuring the mean head width and spine length fluctuation at 1-min intervals. Fluctuation percentages were averaged to give a motility index for cells overexpressing gelsolin-GFP or EGFP. No significant change in spine length or width fluctuation was observed (width: control: 16.3%, gelsolin: 15.1%; length: control: 16%, gelsolin 12.3%). Data are pooled from two independent experiments.

state, we overexpressed gelsolin-GFP in hippocampal neurons for 48 h before fixing them at DIV15. Dendritic spine density and morphology were then analyzed. The total density, as well as distribution of spine types, were all similar in gelsolin-overexpressing neurons compared to control neurons expressing GFP (Figure 4A, B). The only significant change was observed in mushroom spine width; gelsolin-overexpressing neurons had bigger mushroom spines on average (wt 0.60 ± 0.02 μm, gelsolin OE 0.64 ± 0.01 μm). The length of all classes of spines was slightly decreased, as published earlier (Hu and Hsueh, 2014), but these changes were not significant.

We also determined whether gelsolin overexpression affects spine dynamics. Gelsolin overexpression seemed to slightly decrease the dynamics. Gelsolin overexpression especially decreased changes in spine length, but none of these changes were statistically significant (Figure 4C). Taken together, without certain neuronal stimulus leading to gelsolin activation, gelsolin has minor effects on dendritic spine density, morphology or dynamics.

Discussion

In this study, we showed that gelsolin relocates to dendritic spines upon NMDA-induced cLTD induction while it did not show any relocalization upon cLTP induction or during spontaneous activity or upon mGluR agonist induced Ca^{2+}-independent LTD induction. These results support earlier evidence that gelsolin is involved in LTD formation or maintenance (Furukawa et al., 1997; Star et al., 2002). Although the data in the literature is scattered, most of the data point to Ca^{2+}-dependent regulation of gelsolin, and its involvement in actin and LTD regulation. The most plausible, but not yet clear, mechanism for LTD induced relocalization of gelsolin, is that LTD-induced long elevation in Ca^{2+} concentration opens gelsolin's structure, which increases its affinity to F-actin. It is possible that, because all of gelsolin's six domains bind Ca^{2+}, gelsolin structure is opened stepwise. Thus, to open it effectively and achieve full affinity for F-actin, the increase in Ca^{2+} concentration needs to last long enough. It is roughly estimated that the LTD-induced increase in Ca^{2+} concentration lasts for 1 min (in our cLTD induction, it lasted 4 min), whereas for LTP induction, it only lasts a few seconds (Yang et al., 1999) (in our cLTP induction, with relatively low frequency imaging, it lasted less than 2 min). During spontaneous activity, Ca^{2+} concentration increases shortly (under 2–3 s) in various single spines. As F-actin is mainly located in dendritic spines on neuronal dendrites, increased affinity to F-actin would relocate gelsolin from the shaft to spines. Gelsolin did not interact with

postsynaptic density structures, thus it is plausible that its function is to modulate the actin cytoskeleton around synaptic structures, and not the synaptic structures per se. It is expected that binding to F-actin leads to the severing of filaments and thus a decrease in the level of F-actin in spines. A decrease in the amount of F-actin would then facilitate spine shrinkage connected to LTD (Zhou et al., 2004).

We used GFP- or mCherry-labeled exogenously expressed gelsolin for the experiments elucidating the intensity changes in the shaft and spines. The main reason for this was that we mostly used live cell time-lapse imaging in these experiments. In addition, the reason for using gelsolin-GFP in fixed cells (Figure 2A) was that free gelsolin is reported to be difficult to fix (Cooper et al., 1988). Probably due to this fact, it seemed that gelsolin stained with anti-gelsolin antibody was mostly located in spines already at basal conditions. If the free gelsolin is lost during fixation, we cannot detect free shaft gelsolin, which we see in basal conditions with over-expressed gelsolin-GFP. Also with gelsolin-GFP, we saw relatively less gelsolin in the shaft after fixation than in live cells (unpublished observations). Another reason to see changes with gelsolin-GFP but not with endogenous gelsolin is that excess (overexpressed) gelsolin is maybe mostly free in cells. However, earlier results show that also endogenous gelsolin relocates from shaft to dendrites upon glutamate treatment, similar to gelsolin-GFP (Zhao, 2003). We also used anti-gelsolin antibody staining for the experiments elucidating the subcellular localization of the gelsolin compared to synaptic markers (Figure 3C, D). The overexpression of gelsolin resulted in minor effects on dendritic spine density, morphology and dynamics in the resting state. Gelsolin-overexpressing neurons had bigger mushroom spines and the length of all classes of spines were slightly decreased, as published earlier (Hu and Hsueh, 2014). Therefore, it seems that gelsolin is relatively inactive in resting neurons with low concentration of Ca^{2+}.

In the future, it would be interesting to clarify molecular mechanisms leading to gelsolin re-localization to spines upon cLTD induction and to determine how gelsolin is involved in the cLTD-induced effects on F-actin and spine size.

Materials and methods

Plasmid construction

The mCherry-C1 and EGFP plasmids used in our experiments were purchased from Clontech Laboratories Inc. (Mountain View, CA, USA). The pGP-CMV-GCaMP6f was a gift from Douglas Kim (Addgene plasmid #

40755), Lifeact-RFP was kindly provided by Roland Wedlich-Soldner (Riedl et al., 2008) and pCI-SEP-GluR1 was a gift from Robert Malinow (Addgene plasmid # 24000). The mCherry-UtrCH was a gift from William Bement (Addgene plasmid # 26740), gelsolin-GFP was a gift from Pekka Lappalainen. To generate gelsolin-mCherry, the gelsolin-coding sequence was transferred from gelsolin-GFP to an mCherry-C1 vector using standard molecular biological tools (Zheng et al., 2004).

Neuronal cultures, transfections, immunofluorescence and fixed sample preparation

Here, we used primary rat hippocampal neuronal cultures that were prepared as previously described (Bertling et al., 2012). Animals were handled in accordance with Finnish laws and ethics under the EU directive 2010/63/EU. The hippocampi of embryonal day 17 Wistar rat fetuses of either sex were dissected and brains obtained. The meninges were then removed and hippocampi isolated, cells were dissociated with 0.05% papain (Sigma-Aldrich, St. Louis, MO, USA) and mechanical trituration. The cells were plated on coverslips (diameter 13 mm or 18 mm) coated with 0.1 mg/ml Poly-L-Lysine (Sigma-Aldrich, St. Louis, MO, USA) at a density of 75 000/cm^2 and cultured in Neurobasal medium (Gibco™, Thermofisher Scientific, Waltham, MA, USA) supplemented with B-27 (Invitrogen, Thermofisher Scientific, Waltham, MA, USA), L-glutamine (Invitrogen, Thermofisher Scientific, Waltham, MA, USA) and penicillin-streptomycin (Lonza, Basel, Switzerland). Transient transfections were performed, as described earlier (Hotulainen et al., 2009), on DIV17-20, using Lipofectamine 2000 (Invitrogen, Thermofisher Scientific, Waltham, MA, USA). After 24–48 h of expression neurons were either imaged live or fixed on DIV 21 with 4% PFA (Institute of Biotechnology, Media Kitchen, University of Helsinki, Finland) for 12 min.

Live cell imaging

Hippocampal cultured neurons were transfected with gelsolin-GFP or gelsolin-mCherry along with either mCherry, Lifeact-RFP, GluA1-SEP, or GCaMP6f using Lipofectamine 16–24 h before the experiment. Images were made using the 63× oil-immersion objective lens of an inverted Zeiss LSM 880 confocal laser scanning microscope (ZEISS, Oberkochen, Germany) at 37°C. Cells were bathed in HEPES buffered saline (HBS) comprising (in mM): NaCl (115); KCl (5); CaCl2 (2); MgCl2 (2); HEPES (10); D-glucose (10) (Institute of Biotechnology, Media Kitchen, University of Helsinki, Finland); tetrodotoxin citrate (0.5 μM) (Abcam, Cambridge, UK); picrotoxin (50 μM) (Abcam, Cambridge, UK); strychnine (1 μM) (Sigma-Aldrich, St. Louis, MO, USA); pH adjusted to 7.33 with NaOH. To induce chemical NMDAR-dependent LTD the bathing solution was replaced for 4 min with HBS comprising (in mM): NaCl (120); KCl (5); CaCl2 (1.3); HEPES (10); D-glucose (10); tetrodotoxin citrate (0.5 μM); picrotoxin (50 μM); strychnine (1 μM); glycine (1 μM) (Sigma-Aldrich, St. Louis, MO, USA); NMDA (50 μM) (Sigma-Aldrich, St. Louis, MO, USA); pH adjusted to 7.33 with NaOH. To induce chemical mGluR-dependent LTD the bathing solution was replaced for 7 min with HBS comprising (in mM): NaCl (115); KCl (5); CaCl2 (2); MgCl2 (2); HEPES (10); D-glucose (10); tetrodotoxin citrate (0.5 μM); picrotoxin (50 μM); strychnine (1 μM); DHPG (100 μM) (Hello Bio, Bristol, UK); pH adjusted to 7.33 with NaOH. For the cLTP experiments cells were bathed in HEPES buffered saline (HBS) comprising (in mM): NaCl (120); KCl (5); CaCl2 (1.3); HEPES (10);

D-glucose (10); tetrodotoxin citrate (0.5 μM); picrotoxin (50 μM); strychnine (1 μM); pH adjusted to 7.33 with NaOH. To induce chemical LTP the bathing solution was replaced for 4 min with HBS comprising (in mM): NaCl (120); KCl (5); CaCl2 (1.3); HEPES (10); D-glucose (10); tetrodotoxin citrate (0.5 μM); picrotoxin (50 μM); strychnine (1 μM); glycine (200 μM); pH adjusted to 7.33 with NaOH.

Super-resolution sample preparation and imaging

For super-resolution imaging, the neurons were plated on high precision 13 mm glasses at 13 000/cm² density. Cells were fixed with 4% PFA, permeabilized with 0.2% TritonX-100 (Sigma-Aldrich, St. Louis, MO, USA) in PBS for 10 min and then blocked with 3% normal donkey serum (Biowest, Nuaillé, France) and 0.5% bovine serum albumin (BSA, Biotop Oy, Turku, Finland) in phosphate-buffered saline (PBS) for 30 min. Antibodies were diluted separately in blocking solution at 1:200 for primary anti-gelsolin antibody (mouse, BD Biosciences, Franklin Lakes, NJ, USA), PSD95 (rabbit, Cell Signaling Technology, Danvers, MA, USA) or Synapsin-I (rabbit, Covance, Princeton, NJ, USA) and 1:200 for secondary Alexa-488 (anti-mouse, Molecular probes, Thermofisher Scientific, Waltham, MA, USA) or Alexa-647 (anti-rabbit, Invitrogen, Thermofisher Scientific, Waltham, MA, USA), and subsequently 25 μl were dropped onto a parafilm that was then covered by the coverslip. Primary gelsolin antibody was incubated overnight at 4°C, the rest were incubated for 1 h at room temperature. The coverslips were washed 3 times for 10 min with 0.2% BSA in PBS after each incubation, then mounted on microscope slides using ProLong Gold (Invitrogen, Thermofisher Scientific, Waltham, MA, USA). The 3D-SIM images were obtained with the DeltaVision OMX SR imaging system (GE Lifesciences, Marlborough, MA, USA).

Fixed sample imaging and protein localization analysis

Imaging was performed on either a Zeiss LSM880 inverted confocal microscope. A 63 × 1.4 NA oil immersion objective lens and Immersol 518F (ZEISS, Oberkochen, Germany) immersion oil were used to image the fixed samples. For each neuron, a z-stack of 20–30 optical sections was obtained with 0.2–0.3-μm step in the z axis and a pixel size of 0.066 × 0.066 μm for one to two dendritic segments. Image files were processed with Zeiss ZEN (ZEISS, Oberkochen, Germany), LAS AF (Leica, Wetzlar, Germany) and Fiji software (Schindelin et al., 2012, 2015). Fiji software was used to calculate spine-to-dendrite intensity ratios. First, three-dimensional (3D) image data was converted to two-dimensional (2D) using Z-projection based on maximum intensity. To measure the ratio, the average intensity of fluorescence for the protein of interest was measured from a circular region of interest (ROI) in the spine head and compared to the average fluorescence intensity of the equal-sized ROI in the adjacent dendrite. The result was normalized to the intensity distribution of mCherry in the same ROIs. For each neuron 10–20 spines were analyzed. Therefore, for each group we analyzed 90–240 spines.

Statistics

Statistical analysis was performed with the SPSS Statistics (IBM, Armonk, NY, USA) software package and MathWorks MATLAB 2018a (MathWorks, Natick, MA, USA). To examine the differences between separate timepoints in live-cell imaging we used the Wilcoxon signed-rank test. To examine the group differences among the fixed sample data we used the Kruskal-Wallis test.

References

Abraham, W.C. (2008). Metaplasticity: tuning synapses and networks for plasticity. Nat. Rev. Neurosci. *9*, 387.

Anderson, R.G., Falck, J.R., Goldstein, J.L., and Brown, M.S. (1984). Visualization of acidic organelles in intact cells by electron microscopy. Proc. Natl. Acad. Sci. U.S.A. *81*, 4838–4842.

Bertling, E., Ludwig, A., Koskinen, M., and Hotulainen, P. (2012). Methods for three-dimensional analysis of dendritic spine dynamics. Methods Enzymol. *506*, 391–406.

Burkel, B.M., von Dassow, G., and Bement, W.M. (2007). Versatile fluorescent probes for actin filaments based on the actin-binding domain of utrophin. Cell Motil. Cytoskeleton *64*, 822–832.

Chen, C.-C., Lu, J., and Zuo, Y. (2014). Spatiotemporal dynamics of dendritic spines in the living brain. Front. Neuroanat. *8*, 28.

Cooper, J.A., Loftus, D.J., Frieden, C., Bryan, J., and Elson, E.L. (1988). Localization and mobility of gelsolin in cells. J. Cell Biol. *106*, 1229–1240.

Fitzjohn, S.M., Pickard, L., Duckworth, J.K., Molnar, E., Henley, J.M., Collingridge, G.L., and Noël, J. (2001). An electrophysiological characterisation of long-term potentiation in cultured dissociated hippocampal neurones. Neuropharmacology *41*, 693–699.

Forscher, P. (1989). Calcium and polyphosphoinositide control of cytoskeletal dynamics. Trends Neurosci. *12*, 468–474.

Fujii, S., Tanaka, H., and Hirano, T. (2018). Suppression of AMPA receptor exocytosis contributes to hippocampal LTD. J. Neurosci. *38*, 5523–5537.

Furukawa, K., Fu, W., Li, Y., Witke, W., Kwiatkowski, D.J., and Mattson, M.P. (1997). The actin-severing protein gelsolin modulates calcium channel and NMDA receptor activities and

vulnerability to excitotoxicity in hippocampal neurons. J. Neurosci. *17*, 8178–8186.

Halpain, S., Hipolito, A., and Saffer, L. (1998). Regulation of F-actin stability in dendritic spines by glutamate receptors and calcineurin. J. Neurosci. *18*, 9835–9844.

Hanson, J.E. and Madison, D.V. (2010). Imbalanced pattern completion vs. separation in cognitive disease: network simulations of synaptic pathologies predict a personalized therapeutics strategy. BMC Neurosci. *11*, 96.

Hayama, T., Noguchi, J., Watanabe, S., Takahashi, N., Hayashi-Takagi, A., Ellis-Davies, G.C.R., Matsuzaki, M., and Kasai, H. (2013). GABA promotes the competitive selection of dendritic spines by controlling local Ca^{2+} signaling. Nat. Neurosci. *16*, 1409–1416.

Hlushchenko, I., Koskinen, M., and Hotulainen, P. (2016). Dendritic spine actin dynamics in neuronal maturation and synaptic plasticity. Cytoskeleton *73*, 435–441.

Holtmaat, A. and Svoboda, K. (2009). Experience-dependent structural synaptic plasticity in the mammalian brain. Nat. Rev. Neurosci. *10*, 647–658.

Hotulainen, P., Llano, O., Smirnov, S., Tanhuanpää, K., Faix, J., Rivera, C., and Lappalainen, P. (2009). Defining mechanisms of actin polymerization and depolymerization during dendritic spine morphogenesis. J. Cell Biol. *185*, 323–339.

Hu, H. and Hsueh, Y. (2014). Calcium influx and postsynaptic proteins coordinate the dendritic filopodium-spine transition. Dev. Neurobiol. *74*, 1011–1029.

Kinosian, H.J., Newman, J., Lincoln, B., Selden, L.A., Gershman, L.C., and Estes, J.E. (1998). Ca2+ regulation of gelsolin activity: binding and severing of F-actin. Biophys. J. *75*, 3101–3109.

Kleppisch, T., Voigt, V., Allmann, R., and Offermanns, S. (2001). G(alpha)q-deficient mice lack metabotropic glutamate receptor-dependent long-term depression but show normal long-term potentiation in the hippocampal CA1 region. J. Neurosci. *21*, 4943–4948.

Li, Z., Jo, J., Jia, J., Lo, S., Whitcomb, D.J., Cho, K., and Sheng, M. (2010). Caspase-3 activation via mitochondria is required for long-term depression and AMPA receptor internalization. Cell *141*, 859–871.

Li, G.H., Arora, P.D., Chen, Y., McCulloch, C.A., and Liu, P. (2012). Multifunctional roles of gelsolin in health and diseases. Med. Res. Rev. *32*, 999–1025.

Lu, W., Man, H., Ju, W., Trimble, W.S., MacDonald, J.F., and Wang, Y.T. (2001). Activation of synaptic NMDA receptors induces membrane insertion of new AMPA receptors and LTP in cultured hippocampal neurons. Neuron *29*, 243–254.

Malinow, R. and Malenka, R.C. (2002). AMPA receptor trafficking and synaptic plasticity. Annu. Rev. Neurosci. *25*, 103–126.

Miesenböck, G., De Angelis, D.A., and Rothman, J.E. (1998). Visualizing secretion and synaptic transmission with pH-sensitive green fluorescent proteins. Nature *394*, 192–195.

Morishita, W., Marie, H., and Malenka, R.C. (2005). Distinct triggering and expression mechanisms underlie LTD of AMPA and NMDA synaptic responses. Nat. Neurosci. *8*, 1043–1050.

Moult, P.R., Gladding, C.M., Sanderson, T.M., Fitzjohn, S.M., Bashir, Z.I., Molnar, E., and Collingridge, G.L. (2006). Tyrosine phosphatases regulate AMPA receptor trafficking during metabotropic glutamate receptor-mediated long-term depression. J. Neurosci. *26*, 2544–2554.

Nag, S., Larsson, M., Robinson, R.C., and Burtnick, L.D. (2013). Gelsolin: the tail of a molecular gymnast. Cytoskeleton *70*, 360–384.

Okamoto, K.-I., Nagai, T., Miyawaki, A., and Hayashi, Y. (2004). Rapid and persistent modulation of actin dynamics regulates postsynaptic reorganization underlying bidirectional plasticity. Nat. Neurosci. *7*, 1104–1112.

Riedl, J., Crevenna, A.H., Kessenbrock, K., Yu, J.H., Neukirchen, D., Bista, M., Bradke, F., Jenne, D., Holak, T.A., Werb, Z., et al. (2008). Lifeact: a versatile marker to visualize F-actin. Nat. Methods *5*, 605–607.

Sanderson, T.M., Collingridge, G.L., and Fitzjohn, S.M. (2011). Differential trafficking of AMPA receptors following activation of NMDA receptors and mGluRs. Mol. Brain *4*, 30.

Schindelin, J., Arganda-Carreras, I., Frise, E., Kaynig, V., Longair, M., Pietzsch, T., Preibisch, S., Rueden, C., Saalfeld, S., Schmid, B., et al. (2012). Fiji: an open-source platform for biological-image analysis. Nat. Methods *9*, 676–682.

Schindelin, J., Rueden, C.T., Hiner, M.C., and Eliceiri, K.W. (2015). The ImageJ ecosystem: An open platform for biomedical image analysis. Mol. Reprod. Dev. *82*, 518–529.

Star, E.N., Kwiatkowski, D.J., and Murthy, V.N. (2002). Rapid turnover of actin in dendritic spines and its regulation by activity. Nat. Neurosci. *5*, 239–246.

Tanaka, J. and Sobue, K. (1994). Localization and characterization of gelsolin in nervous tissues: gelsolin is specifically enriched in myelin-forming cells. J. Neurosci. *14*, 1038–1052.

Yang, S.-N., Tang, Y.-G., and Zucker, R.S. (1999). Selective induction of LTP and LTD by postsynaptic [Ca^{2+}]$_i$ elevation. J. Neurophysiol. *81*, 781–787.

Zhao, P. (2003). Gelsolin – a regulator of postsynaptic actin assembly and AMPA receptor expression (University of Basel), PhD Thesis. doi:10.5451/unibas-003354194.

Zheng, L., Baumann, U., and Reymond, J.-L. (2004). An efficient one-step site-directed and site-saturation mutagenesis protocol. Nucleic Acids Res. *32*, e115.

Zhou, Q., Homma, K.J., and Poo, M. (2004). Shrinkage of dendritic spines associated with long-term depression of hippocampal synapses. Neuron *44*, 749–757.